LANGMUIR

pubs.acs.org/Langmuir Article

Chain-Length Dependence of Peptide–Lipid Bilayer Interaction Strength and Binding Kinetics: A Combined Theoretical and Experimental Approach

Ryan S. Smith,[§] Dylan R. Weaver,[§] Gavin M. King,* and Ioan Kosztin*

Cite This: https://doi.org/10.1021/acs.langmuir.4c01218 Read Online

ACCESS | Metrics & More | Article Recommendations | Supporting Information

ABSTRACT: Physical interactions between polypeptide chains and lipid membranes underlie critical cellular processes. Yet, despite fundamental importance, key mechanistic aspects of these interactions remain elusive. Bulk experiments have revealed a linear relationship between free energy and peptide chain length in a model system, but does this linearity extend to the interaction strength and to the kinetics of lipid binding? To address these questions, we utilized a combination of coarse-grained molecular dynamics (CG MD) simulations, analytical modeling, and atomic force microscopy (AFM)-based single molecule force spectroscopy. Following previous bulk experiments, we focused on interactions between short hydrophobic peptides (WL_n, n = 1, ..., 5) with 1-palmitoyl-2-oleoyl-glycero-3-phosphocholine (POPC) bilayers, a simple system that probes peptide primary structure effects. Potentials of mean force extracted from CG MD recapitulated the linearity of free energy with the chain length. Simulation results were quantitatively connected to bulk biochemical experiments via a single scaling factor of order unity, corroborating the methodology. Additionally, CG MD revealed an increase in the distance to the transition state, a result that weakens the dependence of the dissociation force on the peptide chain length. AFM experiments elucidated rupture force distributions and, through modeling, intrinsic dissociation rates. Taken together, the analysis indicates a rupture force plateau in the WL_n–POPC system, suggesting that the final rupture event involves the last 2 or 3 residues. In contrast, the linear dependence on chain length was preserved in the intrinsic dissociation rate. This study advances the understanding of peptide–lipid interactions and provides potentially useful insights for the design of peptides with tailored membrane-interacting properties.

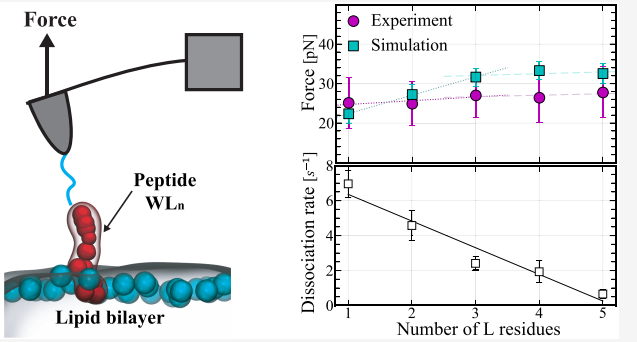

INTRODUCTION

Protein–lipid interactions are fundamental in biology.[1−5] A number of experimental and theoretical techniques have been employed to shed light on these interactions which underlie critical cellular processes and result from a variety of forces including hydrophobic and electrostatic.[6−8] A robust parameter that can be extracted from bulk biochemical assays is the bilayer-to-solution free energy of transfer, ΔG. Seminal work in the field[9] has shown that ΔG increases linearly with peptide chain length for WL_n (n = 1, ..., 5) and POPC, a model system that avoids the complexity of peptide secondary structure formation upon lipid binding. Notwithstanding its importance, free energy is an equilibrium thermodynamic quantity that does not reveal much in terms of mechanistic details at the molecular level. As a result, basic aspects of peptide–lipid interactions, including interaction strength and dissociation kinetics, remain poorly understood.

Computer simulations can provide molecular level mechanistic details that are not accessible to bulk experiments. For example, molecular dynamics (MD) simulations of pentapeptides have aided in interpreting the thermodynamic data that comprises the interfacial hydrophobicity scale developed by Wimley and White.[9−12] One-dimensional free energy profiles, known as the potential of mean force (PMF), have been calculated for side chains of amino acids and short peptides embedded in lipid bilayers.[13−21] Meaningful parameters such as the activation energy (energy barrier height, U_0) and activation length (x_0) can be extracted from this computational method (Figure 1a); however, most investigations have been limited to extracting single PMFs which may not capture the full range of dissociation pathways for peptide–lipid systems. Coarse grain molecular dynamics (CG MD) simulations have proven effective at simulating complex biophysical interac-

Received: April 1, 2024
Revised: June 18, 2024
Accepted: June 18, 2024

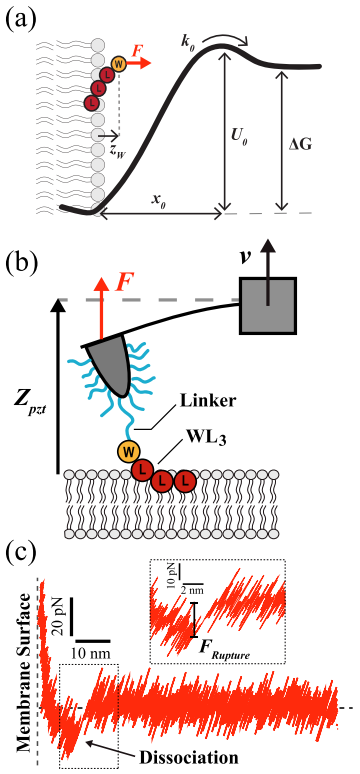

Figure 1. Overview of peptide–lipid dissociation. (a) Forced dissociation of a peptide from a bilayer is modeled as stochastic crossing of a single free energy barrier. The model parameters: activation energy (U_0), activation length (x_0), intrinsic dissociation rate (k_0), and membrane partitioning free energy (ΔG) are shown. The reaction coordinate, z_W, is defined as the normal distance from the membrane surface to the W residue. The experimental observable is force, F, drawn in red. (b) Cartoon of the AFM-based force spectroscopy experiment. (c) Experimental data for WL_3 and POPC. Forced dissociation (rupture) events are marked by a sudden decrease in the force.

tions—such as membrane pore formation,[22] interactions of peripheral membrane and transmembrane proteins,[23] and protein ligand binding[24]—while increasing simulation speed by up to 3 orders of magnitude.[25] The method can provide multiple PMFs per system without undue computational time and is well suited for short peptide chains which do not fold or assume a secondary structure upon binding the membrane.

Mechanistic insights can also be garnered from precise experimental measurements of individual biomolecular interactions. Among single molecule methods, atomic force microscopy (AFM)-based force spectroscopy is well suited for investigations of membrane proteins. Many studies have addressed large membrane protein assemblies, such as bacteriorhodopsin, that are embedded in stable, close-packed arrays.[26−28] Intra- and interprotein interactions are at play in such systems; hence, protein–lipid interactions may not be pronounced. Polypeptide interactions with lipid bilayers under highly dilute conditions have been reported by several groups.[29−31] Experimental rupture force distributions, $P(F)$, generated from repeated approach/retraction experiments revealed that even short peptides (~10 amino acid residues) can display complex behavior when dissociating from lipid membranes. The interactions have been modeled as diffusive escape over a free energy barrier,[32−35] linking the force data to kinetics and requiring complex stochastic models for accurate representation.[36−38]

Here we apply CG MD simulations in conjunction with AFM-based single molecule force spectroscopy to study WL_n (with n = 1, ..., 5) interacting with POPC bilayers. In this system tryptophan (W) effectively anchors the peptide to the bilayer interface and the n leucine (L) residues, which are also hydrophobic, readily penetrate into the lipid bilayer.[13,16,39] This is the same peptide–lipid system utilized by Wimley and White to demonstrate a linear increase in free energy of transfer with leucine number.[9,11] Hence, the system allows quantitative benchmarking to the bulk experimental results. With this work, we sought to characterize the contributions of additional amino acid residues in a peptide chain and thus to quantitatively evaluate the notion of additivity as it pertains to peptide–lipid bilayer interaction strength and dissociation kinetics at the single-molecule level.

RESULTS AND DISCUSSION

Membrane Penetration of Individual WL_n Residues. We used 5 μs long free CG MD simulations to study the partitioning of WL_n into a POPC bilayer (see the Experimental Section for details). In each of the previously equilibrated WL_n–POPC (n = 1, ..., 5) systems, the peptide was placed in the solution at a distance of 1.5 nm above the surface of the bilayer. As expected, within the first 0.5 μs, the peptide partitioned in the membrane. Thus, the last 4.5 μs of the CG MD trajectory was used for the data analysis. The distributions of the membrane penetration depth of individual WL_n residues, shown in Figure 2, provide insight into the conformational dynamics of the partitioned peptide. In Figure 2, the residues are color coded, and each panel refers to a single peptide, starting with WL_1 and ending with WL_5. The plots represent the distribution function, $P(z_{res})$, of the position of the backbone bead of individual residues, z_{res}, with respect to the membrane surface (defined as the plane of the phosphate beads).

All penetration depth distributions are approximately unimodal with similar broadening, as expected for highly mobile, unstructured short peptides. Noticeably, in all WL_n–POPC systems, the terminal W residue has the same mean penetration $z_W \approx -2$ Å, located just below the membrane surface. This observation is consistent with previous experimental and computational findings.[9,10,13,16,40−43]

In all systems, interior L residues exhibit very similar $P(z_{res})$ with peak positions at $z_{res} \approx -3.5$ Å, suggesting that these residues do not go deep into the hydrophobic core of the POPC bilayer. In each system, out of all L residues, the terminal L (which carries a charge) is situated the closest to the surface of the bilayer, with a mean penetration depth similar to that of W, i.e., −2 Å, as shown (Figure 2, black). Thus, the two terminal residues provide a snorkeling conformation[10,18] to WL_n that helps to stabilize it within the POPC bilayer.

Conformational Dynamics of WL_n during Forced Detachment. To mimic the single-molecule forced detachment experiments in which the peptide (tethered to the tip of the AFM cantilever through the terminal W residue) is repeatedly retracted from the surface of the membrane, we used a series of CG steered molecular dynamics (SMD) and equilibrium umbrella sampling (US) simulations that are described in the Experimental Section. Unlike the AFM experiments and the previously described free CG MD

https://doi.org/10.1021/acs.langmuir.4c01218
Langmuir XXXX, XXX, XXX−XXX

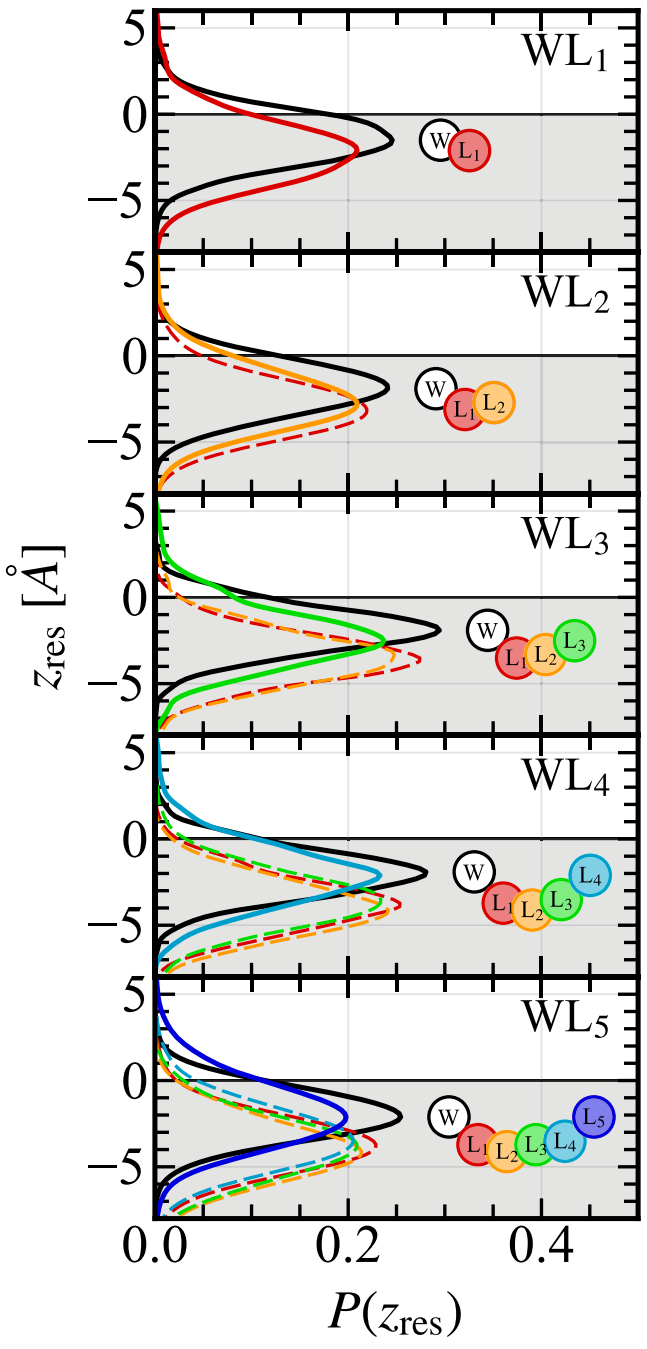

Figure 2. Simulations of penetration depth, z_{res}, distributions, $P(z_{res})$, of individual residues in WL_n (n = 1, ..., 5) partitioned in a POPC bilayer via free CG MD. The shaded gray regions indicate the bilayer interior. The residues are color coded, and their penetration depth distributions are grouped by WL_n peptide, with terminal residues shown in solid lines and interior residues shown as dashed lines. The positions of the residue beads in the cartoons of the individual peptides correspond to their most likely penetration depths.

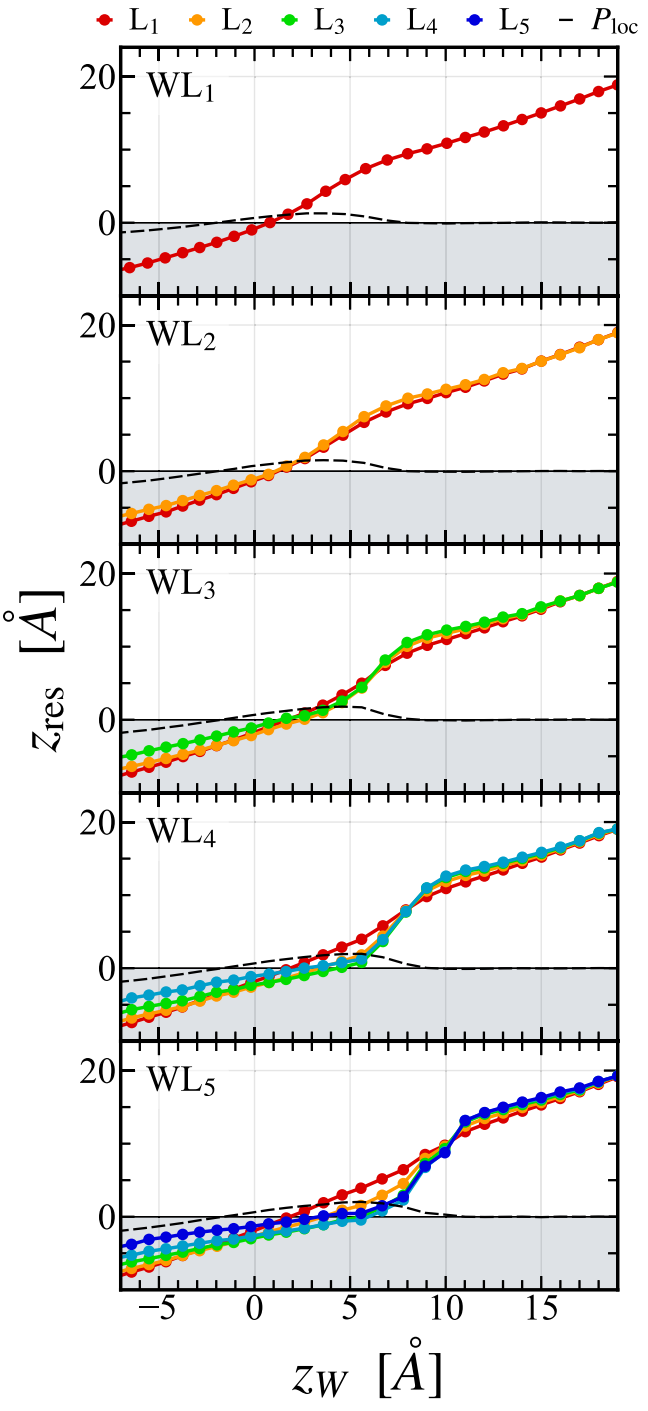

Figure 3. CG US simulation results. Mean position, z_{res}, of individual residues from the surface of the bilayer within each simulated US window as a function of the corresponding target z_W value, for each WL_n peptide. The gray regions represent the interior of the bilayer. The thin-dashed line shows the locally deformed membrane surface (region defined by the phosphates located within a 12 Å radius around the center of mass of the peptide).

simulations, these CG SMD and CG US simulations can provide insight into the order in which the L residues in WL_n detach from the POPC bilayer as W is gradually pulled into the solution along the reaction coordinate, z_W. The CG US simulation results are shown in Figure 3, where the mean positions, z_{res} (measured from the surface of the bilayer, z = 0), of the L residues are plotted as a function of z_W for each WL_n peptide. The plots in Figure 3 suggest that (i) in the membrane-partitioned (z_W < 0) system, the charged terminal L is located closer to the membrane surface than any of the interior L residues; (ii) as W is pulled out of the membrane (z_W > 0), the L residues exit the membrane sequentially, starting with L_1, which is the closest to W; however, (iii) at the very end, for n > 2 (n = 2) the last three (two) L residues leave the surface of the membrane simultaneously. This last

https://doi.org/10.1021/acs.langmuir.4c01218
Langmuir XXXX, XXX, XXX−XXX

observation suggests that the characteristic dissociation force, at least for the peptides considered here, depends only weakly on the length of the peptide.

Furthermore, the CG US simulation results show the peptide−lipid interaction led to only a slight ($\lesssim$2 Å) puckering-like local deformation of the membrane surface (thin-dashed lines in Figure 3) in the proximity of the peptide. In all cases, when the peptide is partitioned (detaching) from the POPC bilayer, these local deformations manifest as a subtle depression (bulging) of the membrane surface.

Potential of Mean Force (PMF). The PMF, $U(z_W)$, represents the free energy profile along the reaction coordinate, z_W, and plays an important role in the quantitative characterization of peptide−lipid interactions. As described in the Experimental Section, for each of the five systems, we reconstructed N_s = 52 PMFs by employing CG US simulations combined with WHAM.[44] Each set of N_s PMFs, corresponding to initial locations of the peptides distributed uniformly throughout the plane of the membrane patch, are plotted in Figure 4 (thin lines). They are all similar and have a simple

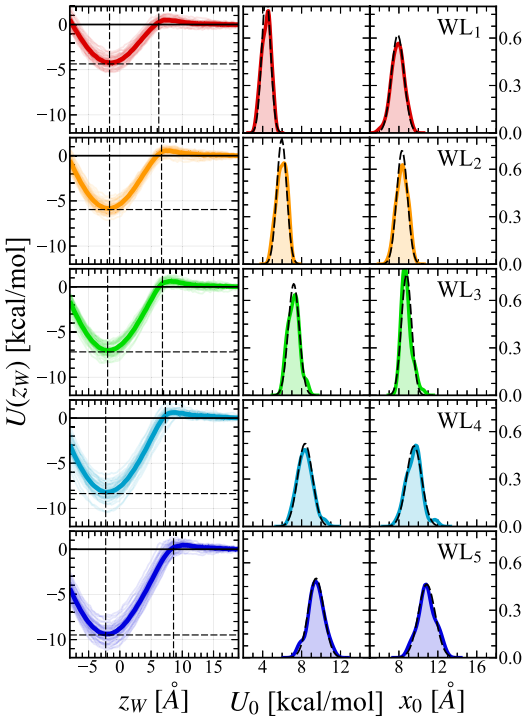

Figure 4. Left column: Ensemble of N_s = 52 PMFs, $U(z_W)$, for each WL_n interacting with a POPC lipid bilayer. The mean PMFs are shown as thick curves. Dashed horizontal and vertical lines indicate the location of the bound and transition states used to calculate the corresponding activation energy U_0 and length x_0. **Right columns:** Distribution functions of the model parameters U_0 and x_0, for each WL_n. They are compared to Gaussian distributions (black dashed lines) defined by the mean and standard deviation values U_0 and x_0, which are listed in Table 1.

structure with a minimum (bound state) and a maximum (transition state), characterized by a free energy barrier (activation energy, U_0) and spatial separation (activation length, x_0). It appears that for all systems the bound state is located around $z_W \approx -2.5$ Å (see also Figure S1), which is consistent with the mean equilibrium position of the W residue in the free CG MD simulations shown in Figure 2. Furthermore, because the distribution functions of U_0 and x_0 are highly peaked and approximately unimodal (see Figure 4), one may conclude that for each WL_n peptide the dissociation from the POPC bilayer takes place along a single energetic pathway defined by the mean PMF (thick curves in Figure 4). The corresponding U_0 and x_0 values (mean and standard deviation) are listed in Table 1. It should be noted that the

Table 1. Mean Values and Standard Deviation of the Activation Energy, U_0 (in kcal/mol), and Activation Length, x_0 (in Å), for WL_n Interacting with POPC Bilayers[a]

WL_n	ΔG	U_0	x_0	F_0	$\bar{F}$
WL_1	3.2	4.4 ± 0.5	7.9 ± 0.6	22.7	22.3
WL_2	3.5	6.0 ± 0.5	8.3 ± 0.6	29.4	27.2
WL_3	4.1	7.2 ± 0.6	8.8 ± 0.5	33.6	31.7
WL_4	4.8	8.4 ± 0.8	9.6 ± 0.8	35.9	33.3
WL_5	5.3	9.5 ± 0.8	10.9 ± 0.9	35.8	32.6

[a]The characteristic dissociation forces, F_0 and $\bar{F}$ (in pN; see the text), are estimates of the peptide−lipid interaction strength. Free energy of transfer from bulk biochemical experiments,[9] ΔG (in kcal/mol), is provided for comparison. Note that for each peptide $\Delta G \approx \tilde{U}_0 = U_0/\alpha$, with $\alpha \approx 1.7$.

values for both U_0 and x_0 increase with the peptide length, n. In fact, as shown in Figure 5, U_0 increases linearly with n, similarly

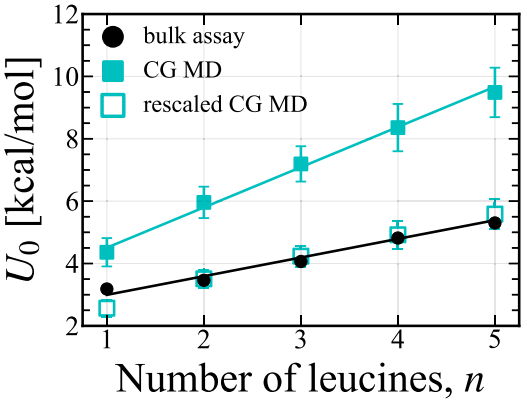

Figure 5. Mean activation energy, U_0 (filled cyan squares), and experimental bulk biochemical free energy of transfer results,[9] ΔG (black circles), as a function of the number of L residues, n. The lines are linear fits through the data points. The rescaled activation energies, $\tilde{U}_0 = U_0/\alpha$ with $\alpha \approx 1.7$ (see text), shown as open cyan squares, align well with the corresponding ΔG values.

to the corresponding free energy of transfer, ΔG, measured in bulk thermodynamic experiments.[9] Interestingly, by rescaling the activation energies, $\tilde{U}_0 = U_0/\alpha$, with the same $\alpha \approx 1.7$, these match closely the experimental ΔG (see Figure 5). Therefore, for subsequent numerical calculations, we have used the rescaled $\tilde{U}_0$ instead of U_0.

Moreover, the PMFs can be used to estimate the characteristic dissociation force, F_d, of the WL_n peptides from the POPC bilayer. Indeed, one can approximate F_d by (1) $F_0 = \tilde{U}_0/x_0$ and (2) $\bar{F} = |\langle d\tilde{U}_0(z_W)/dz_W \rangle|$, where the average is calculated for z_W between the bound and transition states (see also Figure S2). The results for F_d are listed in Table 1, and the values are in the range of 20−30 pN, which are comparable with values reported for similar peptides interacting with lipid membranes.[36−38,45,46] Furthermore, because both U_0 and x_0

https://doi.org/10.1021/acs.langmuir.4c01218
Langmuir XXXX, XXX, XXX−XXX

increase (almost) linearly with the number of L residues, F_d depends only weakly on n, i.e., increases (compared to the n = 1 value) slightly for n = 2, 3 and then levels off for n = 3, 4, 5. This result is consistent with (1) the observation that the final rupture event in the forced dissociation of the peptide involves the last 2 or 3 L residues (see Figure 3) and (2) the AFM force spectroscopy experiments (see below).

Single Molecule Experiments. Experiments were performed to complement the CG MD simulations with real-time, single-molecule data. To this end we performed precision[47] AFM-based force spectroscopy experiments to measure the strength of interaction between each WL_n peptide and POPC bilayers (Figure 1b). AFM tips were functionalized with peptides in a site-specific, covalent manner (see the Experimental Section for details) via a flexible PEG linker.[36,48] Supported POPC lipid bilayers were utilized as robust cellular membrane mimics.[49,50] Figure 1c shows force spectroscopy data for WL_3 dissociating from the bilayer. We note that multiple rupture events on a single trace were sometimes discernible; we recorded the magnitude of the last rupture event (i.e., the event occurring the furthest away from the bilayer surface) in our analyses.

The dissociation force needed to detach a peptide from a lipid membrane is a stochastic quantity and, as such, is characterized by a distribution function $P(F)$, which can be constructed from the AFM force spectroscopy data. $P(F)$, for each WL_n peptide, is shown in Figure S3 and in the top panel of Figure 6. Each $P(F)$ compiles the last rupture events across multiple AFM experiments, with each experiment corresponding to a unique functionalized AFM tip. Table S1 summarizes the number of events collected across all tips used for each peptide along with the number of tips used. Control experiments showed that the majority of dissociation events can be derived from specific peptide−lipid interactions (Figure S4).

The dissociation force distributions in Figure 6 appear to be very similar. Indeed, despite the substantial n-dependence of U_0 and ΔG, the most probable force, F_{MP}, corresponding to the peak of the experimental $P(F)$, increases only slightly with n. Furthermore, because the widths of the $P(F)$s are similar, the corresponding standard deviations are also similar ($\sigma \sim 6$ pN; see Table S1). To better illustrate these observations, the n-dependence of the most probable force F_{MP} is shown in the bottom panel of Figure 6 (filled magenta circles); here the error-bars represent the standard deviation of $P(F)$. For comparison, the n-dependence of the simulated dissociation force $F_d \approx \overline{F} = |\langle d\tilde{U}_0(z_W)/dz_W\rangle|$, calculated from the set of PMFs obtained from CG MD simulations, is also shown (filled cyan squares). While offset slightly higher from the experimental F_{MP}, the simulated F_d has an appreciable n-dependence for $n \leq 3$; i.e., it increases (compared to n = 1) for n = 2, 3 and then levels off for n = 3, 4, 5. A similar n-dependence may also be present in the experimental force data, but the error bars are too large to draw a conclusion. The 13% increase in experimental F_{MP} from about 22 to 25 pN (for n = 1 to n = 5) is within one standard deviation. Line fits through F_{MP} (Figure 6, dotted and dashed lines) guide the eye and do not indicate a statistically significant n-dependence. Taken together, the data suggest that the dissociation force for unstructured lipophilic peptides from lipid bilayers under these conditions is weakly dependent on the length of the peptide.

Theoretical Modeling of $P(F)$. The interactions between the WL_n peptides and POPC membranes are modeled as a diffusive escape over a free energy barrier.[32−35] For each WL_n−POPC system, the dissociation force distribution, $P(F)$, constructed from the AFM data, was fitted using a stochastic model,[37,38,51] as described in the Experimental Section. The model requires as input the (rescaled) PMFs, obtained from CG MD simulations, and uses as fitting parameter the unknown intrinsic dissociation (or off-) rate, k_0. While the dissociation of WL_n from POPC bilayers appears to follow a single dominant pathway (characterized by U_0, x_0, and k_0), the fitting of the AFM data still required the inclusion of double rupture events[38,51] (e.g., when two peptides, bound to the AFM tip, detach simultaneously from the membrane) besides the regular single ruptures (involving the detachment of a single peptide from the membrane; for more details see the Experimental Section). Thus, this requires the introduction of a second fitting parameter, w, representing the fraction of single ruptures ($0 < w < 1$). Furthermore, because the experimental AFM data was poorly sampled at small rupture forces, thus yielding an incomplete $P(F)$ for $F < F_c$ = 15 pN,

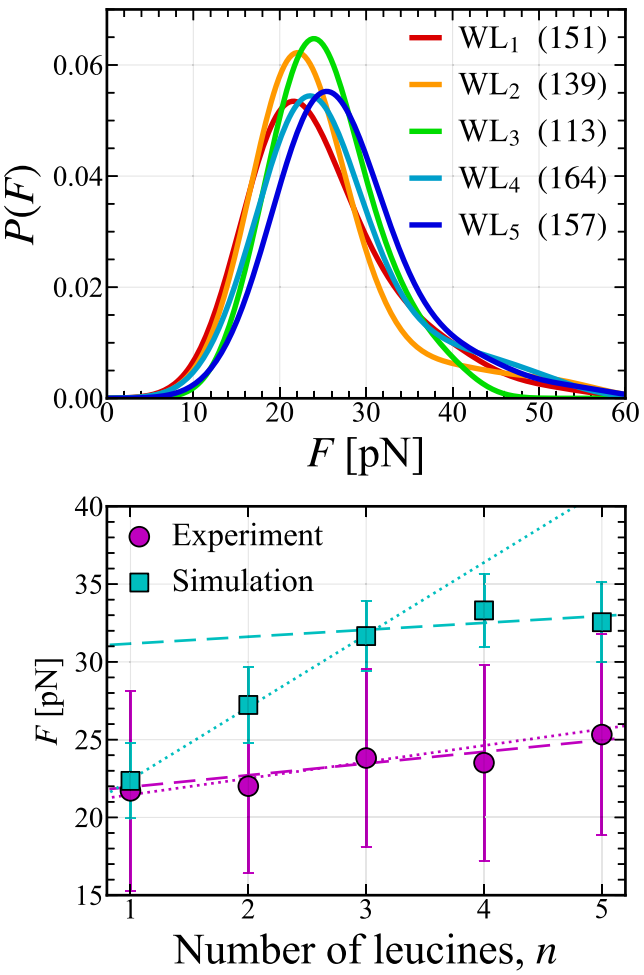

Figure 6. Chain length dependence of the dissociation force. **Top:** Rupture force probability distribution, $P(F)$, for each WL_n (n = 1, ..., 5), obtained from AFM measurements. The number of rupture events included in each distribution is indicated in parentheses. **Bottom:** Most probable (peak) dissociation force corresponding to $P(F)$ (filled magenta circles); the error bar represents the standard deviation of $P(F)$. For comparison, the corresponding forces estimated from the PMFs obtained from CG MD simulations (see Figure S2) are also shown (filled cyan squares). Linear fits of F vs n for n = 1, 2, 3 (dotted lines) and n = 3, 4, 5 (dashed lines) guide the eye.

https://doi.org/10.1021/acs.langmuir.4c01218
Langmuir XXXX, XXX, XXX−XXX

the actual fitting of $P(F)$ was restricted to $F > F_c$. The results of the fittings, including the resulting values of fitting parameters k_0 and w, are shown in Figure 7. By inspection, it is manifest that in general the inclusion of double-rupture events leads to better fits than using only single-ruptures. This conclusion is supported by the smaller χ^2 and BIC values[52,53] for the latter compared to the former (for details, see Table S2). As previously noted,[37,38,51] the theoretical model can extract the $P(F)$ for only single-rupture events (see Figure S5), thus allowing comparisons of seemingly different looking dissociation force distributions obtained from nominally identical experiments. In such cases, the only fitting parameter that is affected is w, which is clearly experiment dependent.

While for the WL_n–POPC systems, both peak and mean values of the dissociation force, as well as the entire $P(F)$ (for single-ruptures) exhibit only a weak n-dependence, the obtained off-rate, k_0, has a significant, near-linear decrease with n, as shown in Figure 8. Each additional L residue reduces the value of k_0 by 1.53 ± 0.22 s^{-1}. Consequently, the intrinsic lipid-bound-state lifetime, $\tau_0 = 1/k_0$, increases faster than linearly with the number of L residues. Thus, for short, unstructured, lipophilic peptides, an increase in chain length leads to only a modest increase in the dissociation force; at the same time, it significantly increases the intrinsic lipid-bound-state lifetime.

CONCLUSIONS

We have presented a quantitative study of the interaction between small lipophilic peptides and a phospholipid bilayer. Our investigation focused on the strength and kinetics of the interaction and explored how these parameters vary with peptide length, as determined by the dissociation force and the intrinsic dissociation rate. A general framework capable of describing peptide–lipid membrane interactions with single residue resolution was employed, which combines CG MD simulations, AFM force spectroscopy experiments, and theoretical modeling.

Experiments were mimicked via tens of μs long CG MD trajectories. These simulations of WL_n interacting with POPC provided crucial insights and, notably, were benchmarked to bulk thermodynamic experiments.[9] The linear increase in free energy of transfer with the number of leucine residues was recapitulated in the simulations. More quantitatively, the rescaled $\tilde{U}_0 = U_0/\alpha$, with $\alpha \approx 1.7$, closely aligned to the bulk experimental ΔG, with each L residue contributing $\Delta\tilde{U}_0 \approx \Delta\Delta G \approx 0.6$ kcal/mol. Importantly, the distance to the transition state, x_0, was also found to increase with n. Since force can be equated to change in energy divided by change in distance, this result renders the mean dissociation force only weakly dependent on the length of the peptide.

Dissociation force distributions were directly measured by AFM-based force spectroscopy. The single molecule experiments revealed a weak interaction strength dependence on n, consistent with the simulation results. For each peptide, we successfully fitted $P(F)$ with a theoretical model[38] that uses simulation-derived U_0 and x_0 as input and intrinsic dissociation rate and weight of single rupture events as fitting parameters. We found that k_0 ranges between ~1 and 7 s^{-1} and decreases approximately linearly with the number of L residues (see Figure 8). This information could be useful for the future design of membrane-cell-interacting peptides with specific mean membrane residency times.

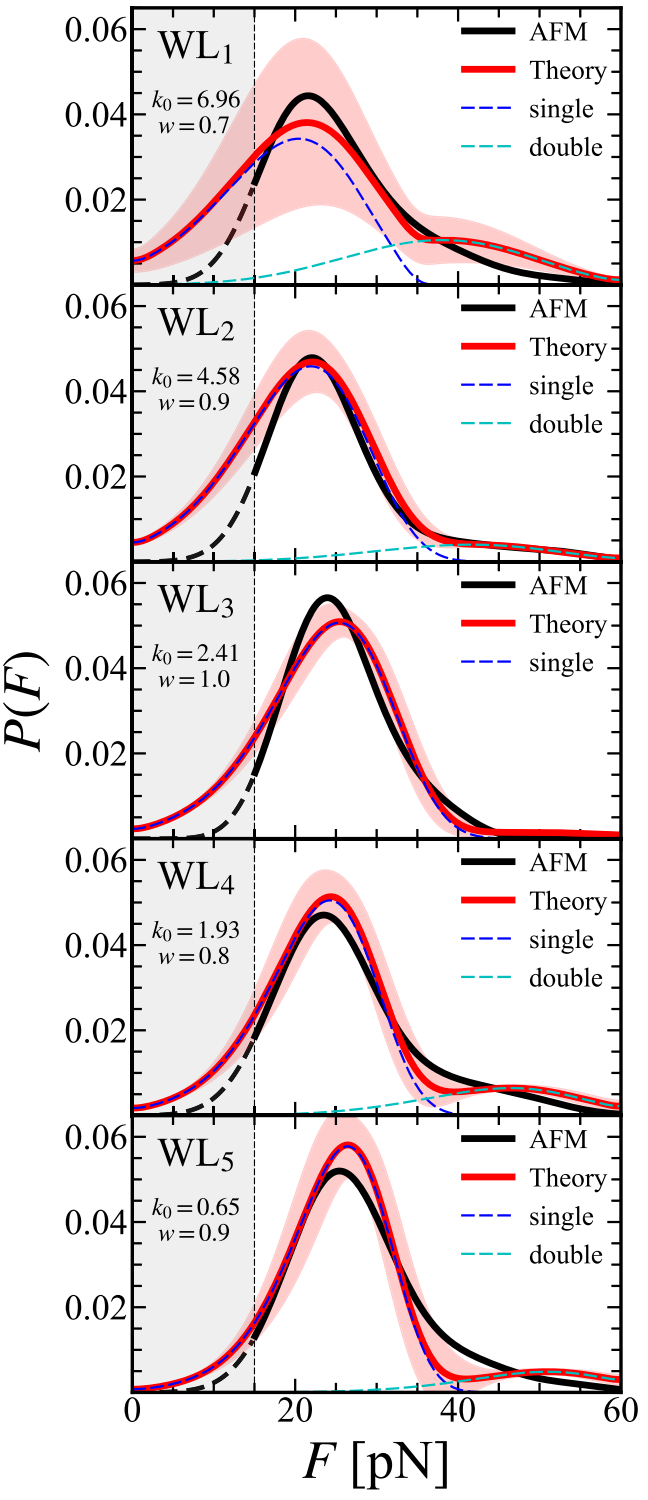

Figure 7. Overlay of experimental (black) and theoretical model (red) dissociation force distributions, $P(F)$'s, for each WL_n peptide. The 1-sigma confidence band of the model $P(F)$ is shown as a pink-shaded region. The gray area indicates the force region undersampled in the experimental data. Contributions from single and double rupture events are shown by dashed blue and cyan lines, respectively. For each fit, the calculated intrinsic off-rate, k_0, and single-rupture weight, w, are also shown.

Taken together, the results indicate that the activation energy (similarly to the free energy of transfer) increases, while the dissociation rate decreases linearly with the number of L

https://doi.org/10.1021/acs.langmuir.4c01218
Langmuir XXXX, XXX, XXX–XXX

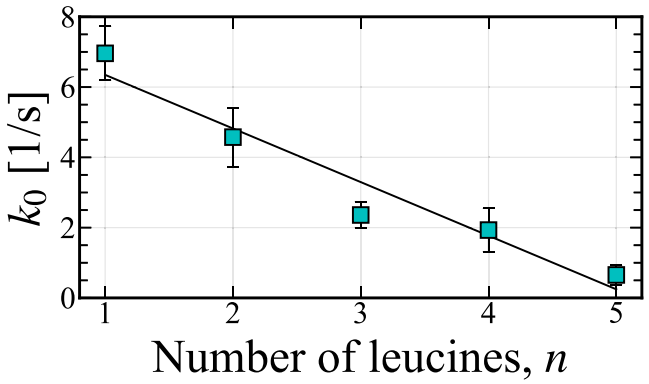

Figure 8. Intrinsic off-rate, k_0, as a function of the peptide length, or number of L residues, n. The error bars represent the standard deviation obtained by using the ensemble of N_s PMFs in the theoretical model $P(F)$ when fitting the experimental $P(F)$.

residues for WL_n interacting with POPC. By contrast, the mean dissociation force (~25 pN) and $P(F)$ depend only weakly on the length of the peptide. We posit that this is because the dissociation events involve only the last few (two or three) L residues, a conjecture that is supported by the CG MD simulations. Further work is required to investigate to what extent these results generalize to peptides with variable residues as well as to longer polypeptide chains that may exhibit higher order structure.

EXPERIMENTAL SECTION

Coarse-Grained Molecular Dynamics Simulations. *System Preparation.* All coarse-grained (CG) WL_n–POPC peptide–lipid bilayer systems were created with CHARMM-GUI Martini Maker.[54,55] The MARTINI[15,56] CG models of the WL_n peptides, with n = 1, ..., 5, were created from atomistic models built with VMD.[57] The CG peptides had a positively (negatively) charged W (L) residue at the N-terminus (C-terminus). The POPC bilayers contained 32 lipids per leaflet and, to mimic experimental conditions,[9] were fully solvated on each side with 25 Å layers of 50 mM NaCl solution. Each WL_n–POPC system comprised around 4,000 CG beads.

Molecular Dynamics Protocol. Simulations were performed in the *NPT* ensemble, using GROMACS 2021.2 with the Martini 2.2 force-field with polarizable water.[15,58,59] Constant pressure (P = 1 atm) was maintained through a semi-isotropic Berendsen barostat, while temperature (T = 300 K) was regulated with the velocity rescaling method, with their respective time constants set at 5 and 1 ps. The systems under these conditions exhibited expected area per lipid (APL ≈ 65 ± 1 Å^2) and bilayer thickness (Δz = 39 ± 1 Å).[60,61] Electrostatic interactions were managed using the reaction field method with an 11 Å cutoff. The equations of motion were integrated using a 20 fs time step.

Constant-velocity steered molecular dynamics (SMD) was used to first guide peptide insertion into the bilayer to z_W = −8 Å. Then, after a 5 μs long constrained equilibration (see below), the peptides were pulled out from the POPC bilayer into solution to z_W = 19 Å. A harmonic guiding potential, with a force constant of 5 kcal/mol·Å^2, was employed for pulling the W backbone beads (z_W) with a speed of 0.1 Å/ns. To account for the local microscopic inhomogeneities of the membrane, N_s = 52 initial configurations, with the location of the residue W distributed uniformly throughout the plane of the membrane patch, were extracted from a 5 μs long CG MD trajectory, in which the W backbone bead was constrained to the deepest insertion of the W residue, i.e., z_W = −8 Å. Each of the subsequent N_s SMD trajectories was 280 ns long.

Potential of Mean Force (PMF) Calculations. PMFs of the WL_n–POPC systems, as a function of the position z_W of the W backbone bead, with respect to the surface of the bilayer (defined as the plane of the phosphate beads) were constructed by using CG umbrella sampling (US), combined with the weighted histogram analysis method (WHAM).[44] For each PMF, N_W = 28 US windows were used, with an adjacent separation of 1 Å and centers located at z_W ranging between −8 and 19 Å. The spring constant for all US simulations was k = 5 kcal/mol·Å^2. For each system, a total of N_s = 52 PMFs were constructed by starting from initial configurations extracted from the corresponding SMD trajectories. In each US window, the reaction coordinate z_W was sampled for 40 ns (over 2 μs) for every (all N_s) PMF calculation(s). Finally, for each system, the mean PMF was calculated by averaging over the N_s PMFs.

Atomic Force Microscopy. *Supported Lipid Bilayer Preparation.* POPC lipid was purchased (Avanti Polar Lipid). Liposomes were prepared by extrusion through a membrane (~25 times, 100 nm pore diameter). Supported lipid bilayers were formed by vesicle fusion (1 mM, 45 min incubation, ~30 °C) to clean glass surfaces, as described previously.[50,62] To verify lipid bilayer coverage we utilized nonfunctionalized cantilevers (AC40, spring constant ~90 pN/nm, Olympus) and performed lipid breakthrough experiments with a tip approach and retraction speed of v = 1000 nm/s (Figure S6).[63,64]

Force Spectroscopy. For force spectroscopy, AFM cantilevers were functionalized following established protocols with minor modifications.[36,48,65] Precision cantilevers with partial reflective coating (qp-SCONT, NanoSensors) were employed.[47] Spring constants were in the range 10–13 pN/nm, as determined via thermal calibration.[66,67] Five distinct peptides were synthesized (Peptide 2.0) at >95% purity with the following sequence C-W-L_n, where n represents the number of leucines in the sequence n = 1, 2, 3, 4, or 5. The cysteine residue at the C-terminus allowed site-specific, covalent binding onto AFM tips via a 9.5 nm long NHS-PEG_{24}-maleimide linker (Thermo Scientific). Cantilevers were oxygen plasma cleaned (10 min, 30 W, Harrick Plasma), immersed in silane (3-ethoxydimethylsilyl) propylamine (Sigma-Aldrich) for 60 s, and baked at 80 °C for 30 min. These dry tips were incubated in sodium borate (50 mM, pH 8.5) for 1 h, followed by the NHS-PEG_{24}-maleimide linker for 1 h, and then peptide at 100 μM for 2 h. Finally, the tips were washed (10 mM HEPES, pH 7.2, 75 mM Na_3PO_4) and loaded into the microscope for force spectroscopy experiments. Such conditions typically yield ~1 peptide tethered to the tip apex.[36] Force spectroscopy experiments were carried out in aqueous buffer solution (100 mM Na_3PO_4, pH 7.6) at ~30 °C using a commercial AFM (Cypher, Asylum Research) with tip retraction speed v = 100 nm/s. To minimize artifacts, the compressive force applied to the lipid bilayer was ≲500 pN. Dissociation events exhibiting rupture forces >60 pN were rare and excluded from analysis. Additionally, to minimize nonspecific interactions, events occurring <3 nm above the lipid surface were excluded from analysis.

Theoretical Modeling of *P*(*F*). Forced detachment of a peptide from a lipid membrane can be described as a stochastic escape process across a free energy barrier.[32−35,68] For each WL_n–POPC system, the dissociation force distribution, $P(F)$, was calculated as[37,38,51]

$$P(F) = \frac{k(F)}{\dot{F}} \exp\left[-\int_0^F \frac{k(f)}{\dot{F}}\,\mathrm{d}f\right] \tag{1}$$

where the force loading rate is $\dot{F} = k_s v$, with cantilever stiffness $k_s \approx 12$ pN/nm and retraction speed v = 100 nm/s, and the force dependent dissociation rate is[38]

$$k(F) = k_0 \frac{\int_{x_-}^{x_+} \mathrm{d}y\, e^{u(y,0)} \int_{-\infty}^{y} \mathrm{d}z\, e^{-u(z,0)}}{\int_{x_-}^{x_+} \mathrm{d}y\, e^{u(y,F)} \int_{-\infty}^{y} \mathrm{d}z\, e^{-u(z,F)}} \tag{2}$$

Here, k_0 is the sought intrinsic dissociation rate, $u(x, F) = (\tilde{U}(x) - Fx)/k_BT$, with $\tilde{U}(x)$ the (rescaled) mean PMF determined from the CG US simulations, k_B the Boltzmann constant, T the temperature, and x_- (x_+) the value of the reaction coordinate z_W in the bound (transition) state corresponding to the minimum (maximum) of the PMF.

https://doi.org/10.1021/acs.langmuir.4c01218
Langmuir XXXX, XXX, XXX−XXX

While our PMF calculations indicate that the dissociation of WL_n from the POPC bilayer occurs along a single dominant energetic pathway (defined by the mean PMF, $\tilde{U}(z)$), in characterizing and fitting the rupture force distribution $P_{exp}(F)$ constructed from the corresponding AFM experimental data, one needs to include both single- and double-rupture events.[38,51] Indeed, the functionalized tip of the AFM cantilever may contain more than one peptide, thus opening the possibility that (within the finite temporal resolution of the AFM instrument) two peptides bound to the bilayer detach simultaneously (double-rupture). In general, the force distribution of double-ruptures, $P_d(F)$, can be calculated as the self-convolution of $P(F)$ for single-ruptures. Indeed, $P_d(F) = \int_0^\infty df_1 \int_0^\infty df_2 P(f_1) P(f_2)\delta(F - f_1 - f_2) = \int_0^F df P(f)P(F - f)$.

Finally, the experimental data was fitted with $P_{exp}(F) = wP(F) + (1 - w)P_d(F)$, where the unknown fraction w of single-rupture events and the intrinsic dissociation rate k_0 were the only fitting parameters.

■ ASSOCIATED CONTENT

Supporting Information

The Supporting Information is available free of charge at https://pubs.acs.org/doi/10.1021/acs.langmuir.4c01218.

Detailed tables quantifying rupture forces and evaluating fit quality for peptide−lipid interactions and additional graphical representations offering insights into the biophysical behavior of these peptides on lipid bilayers (PDF)

■ AUTHOR INFORMATION

Corresponding Authors

Gavin M. King − *Department of Physics & Astronomy, University of Missouri, Columbia, Missouri 65211, United States; Department of Biochemistry, University of Missouri, Columbia, Missouri 65211, United States;* orcid.org/0000-0002-5811-7012; Email: kinggm@missouri.edu

Ioan Kosztin − *Department of Physics & Astronomy, University of Missouri, Columbia, Missouri 65211, United States*; Email: kosztini@missouri.edu

Authors

Ryan S. Smith − *Department of Physics & Astronomy, University of Missouri, Columbia, Missouri 65211, United States*

Dylan R. Weaver − *Department of Physics & Astronomy, University of Missouri, Columbia, Missouri 65211, United States*

Complete contact information is available at: https://pubs.acs.org/10.1021/acs.langmuir.4c01218

Author Contributions

[§]R.S.S., D.R.W.: Contributed equally to this work.

Notes

The authors declare no competing financial interest.

■ ACKNOWLEDGMENTS

This work was supported by the National Science Foundation (NSF) under grant number 2122027. The authors gratefully acknowledge discussions with Dr. Stephen H. White and Dr. Martin B. Ulmschneider.

■ REFERENCES

(1) Phillips, R.; Ursell, T.; Wiggins, P.; Sens, P. Emerging Roles for Lipids in Shaping Membrane-Protein Function. *Nature* **2009**, *459*, 379−385.

(2) Cymer, F.; von Heijne, G.; White, S. H. Mechanisms of Integral Membrane Protein Insertion and Folding. *J. Mol. Biol.* **2015**, *427*, 999−1022.

(3) Copolovici, D. M.; Langel, K.; Eriste, E.; Langel, Ü. Cell-Penetrating Peptides: Design, Synthesis, and Applications. *ACS Nano* **2014**, *8*, 1972−1994.

(4) Nguyen, L. T.; Haney, E. F.; Vogel, H. J. The Expanding Scope of Antimicrobial Peptide Structures and Their Modes of Action. *Trends Biotechnol* **2011**, *29*, 464−472.

(5) White, S. H. Membrane Protein Insertion: The Biology−Physics Nexus. *J. Gen Physiol* **2007**, *129*, 363−369.

(6) White, S. H.; von Heijne, G.; Engelman, D. M. *Cell Boundaries: How Membranes and Their Proteins Work*; Garland Science: 2021.

(7) Simon, S. A., McIntosh, T. J., Eds. *Peptide-Lipid Interactions*, first printing ed.; Academic Press: San Diego, CA, 2002; Vol. *52*.

(8) Scott, J. L.; Musselman, C. A.; Adu-Gyamfi, E.; Kutateladze, T. G.; Stahelin, R. V. Emerging Methodologies to Investigate Lipid−Protein Interactions. *Integr Biol.* **2012**, *4*, 247−258.

(9) Wimley, W. C.; White, S. H. Experimentally Determined Hydrophobicity Scale for Proteins at Membrane Interfaces. *Nat. Struct Mol. Biol.* **1996**, *3*, 842−848.

(10) Aliste, M. P.; Tieleman, D. P. Computer Simulation of Partitioning of Ten Pentapeptides Ace-WLXLL at the Cyclohexane/Water and Phospholipid/Water Interfaces. *BMC Biochem* **2005**, *6*, 30.

(11) Wimley, W. C.; Creamer, T. P.; White, S. H. Solvation Energies of Amino Acid Side Chains and Backbone in a Family of Host-Guest Pentapeptides. *Biochem* **1996**, *35*, 5109−5124.

(12) White, S. H.; Wimley, W. C.; Ladokhin, A. S.; Hristova, K. *Methods in Enzymology*; Energetics of Biological Macromolecules Part B; Academic Press: 1998; Vol. *295*, pp 62−87.

(13) MacCallum, J. L.; Bennett, W. F. D.; Tieleman, D. P. Distribution of Amino Acids in a Lipid Bilayer from Computer Simulations. *Biophys. J.* **2008**, *94*, 3393−3404.

(14) Singh, G.; Tieleman, D. P. Using the Wimley−White Hydrophobicity Scale as a Direct Quantitative Test of Force Fields: The MARTINI Coarse-Grained Model. *J. Chem. Theory Comput* **2011**, *7*, 2316−2324.

(15) de Jong, D. H.; Singh, G.; Bennett, W. F. D.; Arnarez, C.; Wassenaar, T. A.; Schäfer, L. V.; Periole, X.; Tieleman, D. P.; Marrink, S. J. Improved Parameters for the Martini Coarse-Grained Protein Force Field. *J. Chem. Theory Comput* **2013**, *9*, 687−697.

(16) Pogorelov, T. V.; Vermaas, J. V.; Arcario, M. J.; Tajkhorshid, E. Partitioning of Amino Acids into a Model Membrane: Capturing the Interface. *J. Phys. Chem. B* **2014**, *118*, 1481−1492.

(17) Menichetti, R.; Kanekal, K. H.; Kremer, K.; Bereau, T. In Silico Screening of Drug-Membrane Thermodynamics Reveals Linear Relations between Bulk Partitioning and the Potential of Mean Force. *J. Chem. Phys.* **2017**, *147*, 125101.

(18) Hills, R. D., Jr Refining Amino Acid Hydrophobicity for Dynamics Simulation of Membrane Proteins. *PeerJ.* **2018**, *6*, e4230.

(19) Menichetti, R.; Kanekal, K. H.; Bereau, T. Drug−Membrane Permeability across Chemical Space. *ACS Cent Sci.* **2019**, *5*, 290−298.

(20) Hoffmann, C.; Menichetti, R.; Kanekal, K. H.; Bereau, T. Controlled Exploration of Chemical Space by Machine Learning of Coarse-Grained Representations. *Phys. Rev. E* **2019**, *100*, 033302.

(21) Hoffmann, C.; Centi, A.; Menichetti, R.; Bereau, T. Molecular Dynamics Trajectories for 630 Coarse-Grained Drug-Membrane Permeations. *Sci. Data* **2020**, *7*, 51.

(22) Kirsch, S. A.; Böckmann, R. A. Membrane Pore Formation in Atomistic and Coarse-Grained Simulations. *BBA - Biomembranes* **2016**, *1858*, 2266−2277.

(23) Khan, H. M.; Souza, P. C. T.; Thallmair, S.; Barnoud, J.; de Vries, A. H.; Marrink, S. J.; Reuter, N. Capturing Choline−Aromatics Cation-π Interactions in the MARTINI Force Field. *J. Chem. Theory Comput* **2020**, *16*, 2550−2560.

(24) Souza, P. C. T.; Thallmair, S.; Conflitti, P.; Ramírez-Palacios, C.; Alessandri, R.; Raniolo, S.; Limongelli, V.; Marrink, S. J. Protein−Ligand Binding with the Coarse-Grained Martini Model. *Nat. Commun.* **2020**, *11*, 3714.

(25) Bond, P. J.; Holyoake, J.; Ivetac, A.; Khalid, S.; Sansom, M. S. P. Coarse-Grained Molecular Dynamics Simulations of Membrane Proteins and Peptides. *J. Struct Biol.* **2007**, *157*, 593−605.
(26) Oesterhelt, F.; Oesterhelt, D.; Pfeiffer, M.; Engel, A.; Gaub, H. E.; Müller, D. J. Unfolding Pathways of Individual Bacteriorhodopsins. *Science* **2000**, *288*, 143−146.
(27) Yu, H.; Siewny, M. G. W.; Edwards, D. T.; Sanders, A. W.; Perkins, T. T. Hidden Dynamics in the Unfolding of Individual Bacteriorhodopsin Proteins. *Science* **2017**, *355*, 945−950.
(28) Jacobson, D. R.; Perkins, T. T. Free-Energy Changes of Bacteriorhodopsin Point Mutants Measured by Single-Molecule Force Spectroscopy. *Proc. Natl. Acad. Sci. U. S. A.* **2021**, *118*, e2020083118.
(29) Desmeules, P.; Grandbois, M.; Bondarenko, V. A.; Yamazaki, A.; Salesse, C. Measurement of Membrane Binding between Recoverin, a Calcium-Myristoyl Switch Protein, and Lipid Bilayers by AFM-based Force Spectroscopy. *Biophys. J.* **2002**, *82*, 3343−3350.
(30) Takahashi, H.; Shahin, V.; Henderson, R. M.; Takeyasu, K.; Edwardson, J. M. Interaction of Synaptotagmin with Lipid Bilayers, Analyzed by Single-Molecule Force Spectroscopy. *Biophys. J.* **2010**, *99*, 2550−2558.
(31) Schwierz, N.; Krysiak, S.; Hugel, T.; Zacharias, M. Mechanism of Reversible Peptide−Bilayer Attachment: Combined Simulation and Experimental Single-Molecule Study. *Langmuir* **2016**, *32*, 810−821.
(32) Bell, G. I. Models for the Specific Adhesion of Cells to Cells. *Science* **1978**, *200*, 618−627.
(33) Evans, E.; Ritchie, K. Dynamic Strength of Molecular Adhesion Bonds. *Biophys. J.* **1997**, *72*, 1541−1555.
(34) Dudko, O. K.; Hummer, G.; Szabo, A. Intrinsic Rates and Activation Free Energies from Single-Molecule Pulling Experiments. *Phys. Rev. Lett.* **2006**, *96*, 108101.
(35) Dudko, O. K.; Hummer, G.; Szabo, A. Theory, Analysis, and Interpretation of Single-Molecule Force Spectroscopy Experiments. *Proc. Natl. Acad. Sci. U. S. A.* **2008**, *105*, 15755−15760.
(36) Matin, T. R.; Sigdel, K. P.; Utjesanovic, M.; Marsh, B. P.; Gallazzi, F.; Smith, V. F.; Kosztin, I.; King, G. M. Single-Molecule Peptide−Lipid Affinity Assay Reveals Interplay between Solution Structure and Partitioning. *Langmuir* **2017**, *33*, 4057−4065.
(37) Matin, T. R.; Utjesanovic, M.; Sigdel, K. P.; Smith, V. F.; Kosztin, I.; King, G. M. Characterizing the Locus of a Peripheral Membrane Protein-Lipid Bilayer Interaction Underlying Protein Export Activity in E. Coli. *Langmuir* **2020**, *36*, 2143−2152.
(38) Utjesanovic, M.; Matin, T. R.; Sigdel, K. P.; King, G. M.; Kosztin, I. Multiple Stochastic Pathways in Forced Peptide-Lipid Membrane Detachment. *Sci. Rep* **2019**, *9*, 451.
(39) Kanwa, N.; De, S. K.; Maity, A.; Chakraborty, A. Interaction of Aliphatic Amino Acids with Zwitterionic and Charged Lipid Membranes: Hydration and Dehydration Phenomena. *Phys. Chem. Chem. Phys.* **2020**, *22*, 3234−3244.
(40) de Jesus, A. J.; Allen, T. W. The Role of Tryptophan Side Chains in Membrane Protein Anchoring and Hydrophobic Mismatch. *BBA - Biomembranes* **2013**, *1828*, 864−876.
(41) Sun, H.; Greathouse, D. V.; Andersen, O. S.; Koeppe, R. E. The Preference of Tryptophan for Membrane Interfaces: Insights from N-methylation of Tryptophans in Gramicidin Channels. *J. Biol. Chem.* **2008**, *283*, 22233−22243.
(42) Situ, A. J.; Kang, S.-M.; Frey, B. B.; An, W.; Kim, C.; Ulmer, T. S. Membrane Anchoring of α-Helical Proteins: Role of Tryptophan. *J. Phys. Chem. B* **2018**, *122*, 1185−1194.
(43) Khemaissa, S.; Sagan, S.; Walrant, A. Tryptophan, an Amino-Acid Endowed with Unique Properties and Its Many Roles in Membrane Proteins. *Crystals* **2021**, *11*, 1032.
(44) Grossfield, A. An Implementation of WHAM: The Weighted Histogram Analysis Method, version 2.0.10.
(45) Ma, C. D.; Acevedo-Vélez, C.; Wang, C.; Gellman, S. H.; Abbott, N. L. Interaction of the Hydrophobic Tip of an Atomic Force Microscope with Oligopeptides Immobilized Using Short and Long Tethers. *Langmuir* **2016**, *32*, 2985−2995.
(46) Stock, P.; Monroe, J. I.; Utzig, T.; Smith, D. J.; Shell, M. S.; Valtiner, M. Unraveling Hydrophobic Interactions at the Molecular Scale Using Force Spectroscopy and Molecular Dynamics Simulations. *ACS Nano* **2017**, *11*, 2586−2597.
(47) Churnside, A. B.; Sullan, R. M. A.; Nguyen, D. M.; Case, S. O.; Bull, M. S.; King, G. M.; Perkins, T. T. Routine and Timely Sub-picoNewton Force Stability and Precision for Biological Applications of Atomic Force Microscopy. *Nano Lett.* **2012**, *12*, 3557−3561.
(48) Zimmermann, J. L.; Nicolaus, T.; Neuert, G.; Blank, K. Thiol-Based, Site-Specific and Covalent Immobilization of Biomolecules for Single-Molecule Experiments. *Nat. Protoc* **2010**, *5*, 975−985.
(49) Tamm, L. K.; McConnell, H. M. Supported Phospholipid Bilayers. *Biophys. J.* **1985**, *47*, 105−113.
(50) Cremer, P. S.; Boxer, S. G. Formation and Spreading of Lipid Bilayers on Planar Glass Supports. *J. Phys. Chem. B* **1999**, *103*, 2554−2559.
(51) King, G. M.; Kosztin, I. *J. Membr. Biol.* **2021**, *254*, 17.
(52) Schwarz, G. Estimating the Dimension of a Model. *Ann. Stat* **1978**, *6*, 461−464.
(53) Kinz-Thompson, C. D.; Ray, K. K.; Gonzalez, R. L. Bayesian Inference: The Comprehensive Approach to Analyzing Single-Molecule Experiments. *Annu. Rev. Biophys* **2021**, *50*, 191−208.
(54) Jo, S.; Kim, T.; Iyer, V. G.; Im, W. CHARMM-GUI: A Web-Based Graphical User Interface for CHARMM. *J. Comput. Chem.* **2008**, *29*, 1859−1865.
(55) Hsu, P.-C.; Bruininks, B. M. H.; Jefferies, D.; Cesar Telles de Souza, P.; Lee, J.; Patel, D. S.; Marrink, S. J.; Qi, Y.; Khalid, S.; Im, W. CHARMM-GUI Martini Maker for Modeling and Simulation of Complex Bacterial Membranes with Lipopolysaccharides. *J. Comput. Chem.* **2017**, *38*, 2354−2363.
(56) Marrink, S. J.; Risselada, H. J.; Yefimov, S.; Tieleman, D. P.; de Vries, A. H. The MARTINI Force Field: Coarse Grained Model for Biomolecular Simulations. *J. Phys. Chem. B* **2007**, *111*, 7812−7824.
(57) Humphrey, W.; Dalke, A.; Schulten, K. VMD: Visual Molecular Dynamics. *J. Mol. Graph* **1996**, *14*, 33−38.
(58) Yesylevskyy, S. O.; Schäfer, L. V.; Sengupta, D.; Marrink, S. J. Polarizable Water Model for the Coarse-Grained MARTINI Force Field. *PLOS Comput. Biol.* **2010**, *6*, e1000810.
(59) Abraham, M. J.; Murtola, T.; Schulz, R.; Páll, S.; Smith, J. C.; Hess, B.; Lindahl, E. GROMACS: High Performance Molecular Simulations through Multi-Level Parallelism from Laptops to Supercomputers. *SoftwareX* **2015**, *1−2*, 19−25.
(60) Kučerka, N.; Tristram-Nagle, S.; Nagle, J. F. Structure of Fully Hydrated Fluid Phase Lipid Bilayers with Monounsaturated Chains. *J. Membr. Biol.* **2006**, *208*, 193−202.
(61) Hills, R. D.; McGlinchey, N. Model Parameters for Simulation of Physiological Lipids. *J. Comput. Chem.* **2016**, *37*, 1112−1118.
(62) Chada, N.; Sigdel, K. P.; Gari, R. R. S.; Matin, T. R.; Randall, L. L.; King, G. M. Glass Is a Viable Substrate for Precision Force Microscopy of Membrane Proteins. *Sci. Rep* **2015**, *5*, 12550.
(63) Alessandrini, A.; Seeger, H. M.; Cerbo, A. D.; Caramaschi, T.; Facci, P. What Do We Really Measure in AFM Punch-through Experiments on Supported Lipid Bilayers? *Soft Matter* **2011**, *7*, 7054−7064.
(64) Morandat, S.; Azouzi, S.; Beauvais, E.; Mastouri, A.; El Kirat, K. Atomic Force Microscopy of Model Lipid Membranes. *Anal Bioanal Chem.* **2013**, *405*, 1445−1461.
(65) Sigdel, K. P.; Pittman, A. E.; Matin, T. R.; King, G. M. In *Nanoscale Imaging: Methods and Protocols*; Lyubchenko, Y. L., Ed.; Methods in Molecular Biology; Springer: New York, 2018; pp 49−62.
(66) Higgins, M. J.; Proksch, R.; Sader, J. E.; Polcik, M.; Mc Endoo, S.; Cleveland, J. P.; Jarvis, S. P. Noninvasive Determination of Optical Lever Sensitivity in Atomic Force Microscopy. *Rev. Sci. Instrum.* **2006**, *77*, 013701.
(67) Sader, J. E.; Chon, J. W. M.; Mulvaney, P. Calibration of Rectangular Atomic Force Microscope Cantilevers. *Rev. Sci. Instrum.* **1999**, *70*, 3967−3969.
(68) Hummer, G.; Szabo, A. Kinetics from Nonequilibrium Single-Molecule Pulling Experiments. *Biophys. J.* **2003**, *85*, 5−15.

https://doi.org/10.1021/acs.langmuir.4c01218
Langmuir XXXX, XXX, XXX−XXX